Vol. 107 No. 2 February 2009

Oral Surgery, Oral Medicine, Oral Pathology, Oral Radiology, and Endodontology

ORAL AND MAXILLOFACIAL RADIOLOGY Editor: Allan G. Farman

Observer reliability of three-dimensional cephalometric landmark identification on cone-beam computerized tomography

Ana Emilia F. de Oliveira, DDS, PhD,[a] Lucia Helena S. Cevidanes, DDS, PhD,[b] Ceib Phillips, MPH, PhD,[c] Alexandre Motta, DDS, MS, PhD,[d] Brandon Burke,[e] and Donald Tyndall, DDS, PhD,[f] Maranhão and Rio de Janeiro, Brazil; and Chapel Hill, North Carolina

UNIVERSIDADE FEDERAL DO MARANHÃO, UNIVERSIDADE DO ESTADO DO RIO DE JANEIRO, AND UNIVERSITY OF NORTH CAROLINA

Objective. To evaluate reliability in 3-dimensional (3D) landmark identification using cone-beam computerized tomography (CBCT).

Study design. Twelve presurgery CBCTs were randomly selected from 159 orthognathic surgery patients. Three observers independently repeated 3 times the identification of 30 landmarks in the sagittal, coronal, and axial slices. A mixed-effects analysis of variance model estimated the intraclass correlations (ICC) and assessed systematic bias.

Results. The ICC was >0.9 for 86% of intraobserver assessments and 66% of interobserver assessments. Only 1% of intraobserver and 3% of interobserver coefficients were <0.45. The systematic difference among observers was greater in X and Z than in Y dimensions, but the maximum mean difference was quite small.

Conclusion. Overall, the intra- and interobserver reliability was excellent. Three-dimensional landmark identification using CBCT can offer consistent and reproducible data if a protocol for operator training and calibration is followed. This is particularly important for landmarks not easily specified in all 3 planes of space. **(Oral Surg Oral Med Oral Pathol Oral Radiol Endod 2009;107:256-265)**

Three-dimensional (3D) cephalometry has long been proposed as the ideal for orthodontic diagnosis, treatment planning, and follow-up of the patients.[1] Diagnosis, treatment planning, and assessment of change over time have been routinely based on landmark-based analysis in 2D cephalometry.[1]

Three-dimensional landmarks represent an advantage over traditional location of 2D landmarks, which may be hindered by rotational, geometric, and head-positioning errors.[2,3] These errors may lead to inaccurate representation of anatomic landmarks or poor visualization of some structures.[4] The use of cone-beam computerized tomography (CBCT) in dentistry offers great potential for 3D diagnosis and treatment planning compared with CT.[5-16] However, the development of 3D landmark-based cephalometric analysis requires definition of 3D landmarks on complex curving structures, which is not a trivial problem. As Bookstein[16] noted, there is a lack of literature about suitable operational definitions for the landmarks in the 3 planes of space (coronal, sagittal, and axial). Practical considerations of identification errors, coupled with an essential

Supported by National Institute for Dental and Craniofacial Research (NIDCR) DE017727, DE005215, and Fundaço de Auxílio à Pesquisa do Estado do Maranhão (FAPEMA) 128/06.

[a]Professor, Department of Dentistry—I, Universidade Federal do Maranhão.

[b]Assistant Professor, Department of Orthodontics, University of North Carolina.

[c]Professor, Department of Orthodontics, University of North Carolina.

[d]Department of Orthodontics, Universidade do Estado do Rio de Janeiro.

[e]Fourth-Year DDS Student, University of North Carolina.

[f]Professor, Department of Diagnostic Sciences and General Dentistry, University of North Carolina.

1079-2104/$ - see front matter

doi:10.1016/j.tripleo.2008.05.039

need for biologic relevance and a balanced representation of components of the craniofacial form, limit the number and nature of landmarks available for analysis. Historically, landmarks, such as Articulare, were used because of the ease in landmark location on the 2D cephalometric projections, but these projected superimposed structures do not exist in the actual 3D facial structure. For these reasons, the development of 3D landmark-based cephalometric analysis demands suitable operational definitions of the landmark location in each of the 3 planes of space,[6] and reproducibility of landmark identification is necessary to take full advantage of the 3D diagnostic power offered by CBCT imaging.[17]

If 3D landmark identification is reliable and research protocols are carefully planned to avoid bias, 3D cephalometry has the potential of providing unambiguous information for diagnosis of skeletal asymmetry, longitudinal monitoring of growth, and postsurgical assessment. It is well known that operator experience has a positive effect on measurement accuracy and reproducibility.[17] The purpose of the present article was to evaluate intra- and interobserver reliability in 3D landmark identification using CBCT images.

MATERIAL AND METHODS

Presurgical CBCT images of 12 patients with varying dentofacial deformities (6 skeletal class II and 6 skeletal class III) were randomly selected to represent the spectrum of diverse facial morphologies from an available pool of 159 patients enrolled in parent study in our Dentofacial Deformities Program. The inclusion criteria for enrollment in the parent study were skeletal deformity severe enough to warrant surgical correction and age between 13 and 50 years. The exclusion criteria were: 1) presence of a cleft; 2) problems secondary to trauma; 3) degenerative conditions (e.g., rheumatoid arthritis); 4) pregnancy at baseline; 5) correction by genioplasty only; and 6) inability to follow written English instructions. Patients were not excluded on the basis of age, gender or ethnicity. Biomedical Institutional Review Board was obtained, and informed consent and Health Insurance Portability and Accountability Act (HIPAA) authorization forms were signed by all subjects.

The CBCT scans were obtained using the Dental Volumetric Tomograph NewTom 3G (AFP Imaging, Elmsford, NY). The scanner was operated by a personal computer which used Windows NT operating system (Microsoft Corporation, Redmond, WA). The basis projections were transfered as raw image data to an Expert Workstation, where the primary reconstruction was performed using filtered back projection techniques to build the 3D data volume. Secondary reconstruction was equivalent to multiplanar reformatting, allowing the operator to obtain image slices through the 3D volume in any directions.[18] The imaging protocol used a 12-inch field of view to include the entire facial anatomy. The axial slice thickness was 0.3 mm and the voxels were isotropic. Axial images were saved as 12-bit-depth DICOM files. These images were imported in Dolphin 3D (prerelease version 1; Dolphin Imaging and Management Systems, Chatsworth, CA), which uses the same procedures as the current version of Dolphin 10 for 3D landmark identification. For each subject, a 3D virtual model was created and used to determine head orientation and standardize the center of the 3D coordinate system. Using axial, coronal, and sagittal views of the 3D head rendering, the midsagittal plane of the model was oriented vertically, the transporionic line was oriented horizontally, and the Frankfort horizontal plane was oriented horizontally. The center of the coordinate system was determined by the intersection of the transporionic line and the midsagittal plane.[19]

A total of 30 landmarks were selected (Table I), and defined criteria were established for each landmark. The X, Y, and Z coordinates of each landmark were defined to standardize the anatomic identification in the 3 planes of space and to guide the selection of the most appropriate slice in the axial, coronal, and sagittal views (Figs. 1 and 2). Besides the cross-sectional slices in the 3 planes of space, the Dolphin software also allows visualization of a 3D virtual rendering. The 3D virtual rendering was used to confirm landmark spatial position, but not for landmark location, because 3D renderings are projected images and not actual surfaces (Fig. 3). If the observer had difficulty visualizing any landmark in a specific plane, the software allowed both mutliplanar views or selection of just 1 single plane in full-screen window to zoom and facilitate landmark location (Fig. 3).

Three observers (an orthodontist, a dental radiologist, and a third-year dental student) were trained and calibrated to identify 3D landmarks using the sagittal, coronal, and axial slices using a set of 10 CBCT scans not included in this study. Working independently after calibration, the 3 observers identified and marked the 30 anatomic landmarks in 12 CBCT exams. Using the sagittal, coronal, and axial views, the position of the landmark was recorded by the Dolphin 3D software as numerical values for the X, Y, and Z coordinates, respectively. The digitized data were then exported to a Microsoft Excel spreadsheet (Microsoft Corporation, Redmond, WA). The landmark identifications were repeated 3 times by each observer at intervals of at least 3 days, yielding 36 sets for each observer. A 2-way mixed-effects analysis of variance (ANOVA) model

Table I. Landmarks selected for the study

Landmark name	*Anatomic region*	*Lateral view*	*Axial view*	*Anteroposterior view*
1. Sella turcica (S)	Pituitary fossa of the sphenoidal bone	Middle point of the anteroposterior width of the fossa	Middle point of the anteroposterior and lateral width of the fossa	Middle point of the lateral width of the fossa in the anteroposterior slice determined by the lateral and axial views
2. Nasion (N)	Frontonasal suture	Anterior-most point	Middle-anterior–most point on the anterior contour	Middle point
3. A point (A)	Premaxilla	Posterior-most point on the curve of the maxilla between the anterior nasal spine and supradentale	Middle-anterior–most point on the tip of the premaxilla	Middle point in the anteroposterior slice determined by the lateral and axial views
4. B point (B)	Anterior surface of the mandibular symphysis	Posterior-most point	Middle-anterior–most point on the anterior contour	Middle point in the anteroposterior slice determined by the lateral and axial views
5. Pogonion (Pg)	Contour of the bony chin	Anterior-most point	Middle-anterior–most point on the anterior contour	Middle point in the anteroposterior slice determined by the lateral and axial views
6. Gnathion (Gn)	Contour of the bony chin	Anterior-inferior–most point	Middle-anterior-inferior–most point	Middle-inferior–most point
7. Menton (ME)	Lower border or the mandible	Inferior-most point	Middle-inferior–most point	Inferior-most point
8. Anterior nasal spine (ANS)	Median, sharp bony process of the maxilla	Point on the tip	Anterior-most point	Middle point in the anteroposterior slice determined by the lateral and axial views
9. Right mandibular gonion (rGo)	Angle of the right mandibular body	Middle point along the angle	Posterior-most point	Inferior-most point
10. Left mandibular gonion (lGo)	Angle of the left mandibular body	Middle point along the angle	Posterior-most point	Inferior-most point
11. Right condylion (rCo)	Right condyle	Superior-most point	Middle point in the axial slice level determined by the lateral and anteroposterior views	Middle-superior–most point
12. Left condylion (lCo)	Left condyle	Superior-most point	Middle point in the axial slice level determined by the lateral and anteroposterior views	Middle-superior–most point
13. Right orbitale (rOr)	Lateroinferior contour of the right orbit	Anterior-superior–most point on the edge between the internal and external contours	Anterior-most point	Lateroinferior most point
14. Left orbitale (lOr)	Lateroinferior contour of the left orbit	Anterior-superior–most point on the edge between the internal and external contours	Anterior-most point	Lateroinferior most point
15. Right upper incisal edge I (rUIE)	Incisal tip of right upper central incisor	Inferior-most point	Middle point of the mesiodistal and buccolingual width	Middle point of the mesiodistal width
16. Right lower incisal edge (rLIE)	Incisal tip of right lower central incisor	Superior-most point	Middle point of the mesiodistal and buccolingual width	Middle point of the mesiodistal width

Table I. Continued

Landmark name	*Anatomic region*	*Lateral view*	*Axial view*	*Anteroposterior view*
17. Right lateral mandibular condyle (rLCo)	Lateral contour of the right condyle	Middle point in the lateral slice determined by the axial and anteroposterior views	Middle-lateral–most point on the external surface	Lateral-most point
18. Left lateral mandibular condyle (lLCo)	Lateral contour of the left condyle	Middle point in the lateral slice determined by the axial and anteroposterior views	Middle-lateral–most point on the external surface	Lateral-most point
19. Right medial mandibular condyle (rMCo)	Medial contour of the right condyle	Middle point in the lateral slice determined by the axial and anteroposterior views	Middle-medial-most point on the external surface	Medial-most point
20. Left medial mandibular condyle (lMCo)	Medial contour of the left condyle	Middle point in the lateral slice determined by the axial and anteroposterior views	Middle-medial–most point on the external surface	Medial-most point
21. Right ramus point (rRP)	Posterior border of the right mandibular ramus	Middle-posterior–most point between the condylar neck and the angle of the mandibular body	Middle-posterior–most point	Inferior-most point
22. Left ramus point (lRP)	Posterior border of the left mandibular ramus	Middle-posterior–most point between the condylar neck and the angle of the mandibular body	Middle-posterior–most point	Inferior-most point
23. Right upper molar point (rUM1)	Distal surface of the molar tube	Middle-posterior–most point	Middle-posterior–most point	Lateral-most point
24. Left upper molar point (lUM1)	Distal surface of the molar tube	Middle-posterior–most point	Middle-posterior–most point	Lateral-most point
25. Right lower molar point (rLM1)	Distal surface of the molar tube	Middle-posterior–most point	Middle-posterior–most point	Lateral-most point
26. Left lower molar point (lLM1)	Distal surface of the molar tube	Middle-posterior-most point	Middle-posterior–most point	Lateral-most point
27. Right tuberosity (rTb)	Distal contour of the right maxillary tuberosity	Posterior-inferior–most point	Posterior-most point	Inferior-most point
28. Left tuberosity (lTb)	Distal contour of the left maxillary tuberosity	Posterior-inferior–most point	Posterior-most point	Inferior-most point
29. Right Zygomatic Suture (rZS)	Zygomaticomaxillary suture	Anterior-inferior–most point	Anterior-most point	Lateral-inferior–most point
30. Left zygomatic suture (lZS)	Zygomaticomaxillary suture	Anterior-inferior–most point	Anterior-most point	Lateral-inferior–most point

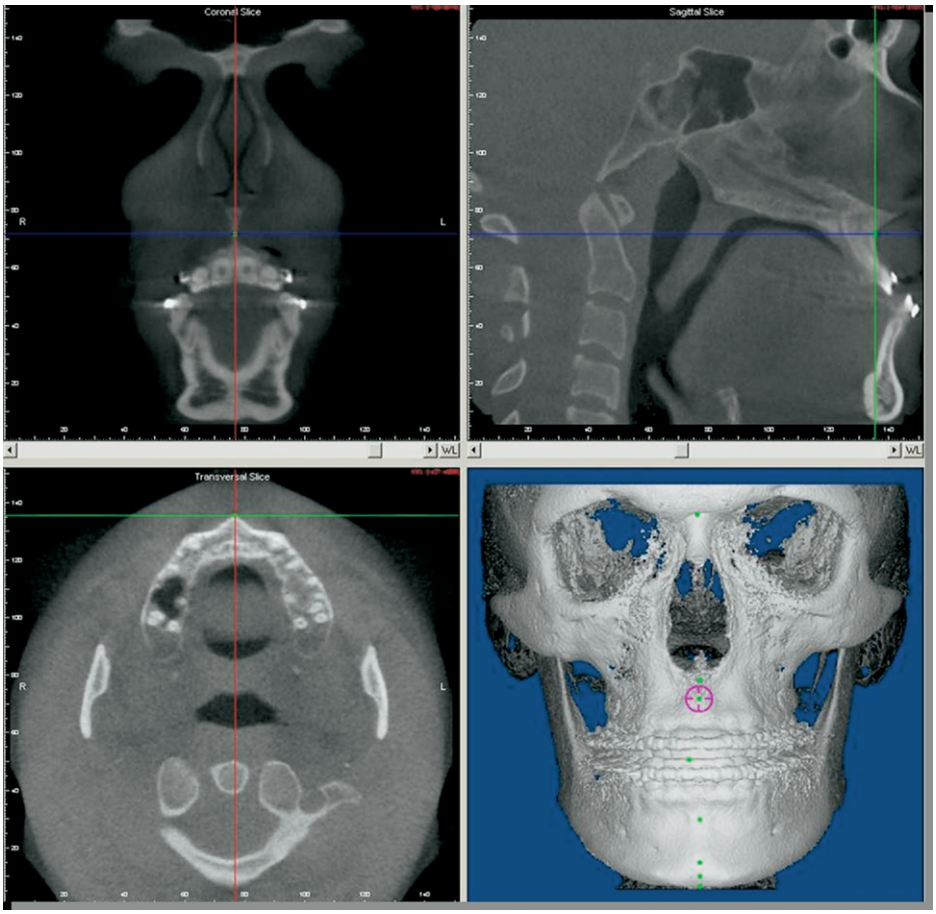

Fig. 1. Example of identification of the A point in the 3 planes of space. The software allows tracking of the cursor with display of all 3 planes of space and 3D rendering in the same software window to verify landmark location.

with an interaction between observer and patient was fitted to each landmark and each coordinate, with observer as a fixed effect (3 levels) and patient as a random effect (12 levels). Intraclass correlation (ICC) formulas were determined using the table of expected mean squares (MS) [20]: ICC within observer = (MSpatient + 3MSinteraction − 4MSerror)/(MSpatient + 3MSinteraction + 5MSError); ICC between observer = (MSpatient − MSError)/(MSpatient + 3MSinteraction + 5MSError). A separate repeated-measures ANOVA model was fitted without the interaction between patient and observer to assess whether bias among the observers existed. To test whether there was systematic bias in the observer estimates of landmark location, that means to test that at least 1 pair of observers had a mean difference significantly different from zero, or that at least 1 observer located a landmark consistently differently: An F test was calculated for the X, Y, and Z coordinates of each landmark. The level of significance was set at .05.

RESULTS

The reliability was estimated by ICC for each landmark and each coordinate. Tables of frequencies of the intra- and interobserver reliability summarize the results (Tables II and III). Overall, these tables show that the ICC indicated excellent reliability for both intra- and interobserver assessments.

Table II shows the frequency of the intraobserver reliability estimated by ICC for the X, Y, and Z coordinates. The ICC was ≥0.9 for 77 (85.55%) of the intraobserver assessments, with the greatest frequency in the Z coordinate (93.33%). Only 1 (1.1%) of the intraobserver coefficients showed poor reliability (ICC <0.45), which also occurred in the Z coordinate.

The frequency of the interobserver reliability estimated by ICC for the X, Y, and Z coordinates are shown in Table III. The ICC was ≥0.9 for 59 (65.55%) of the interobserver assessments with the greatest frequency in the Z coordinate (80.00%). A poor reliability

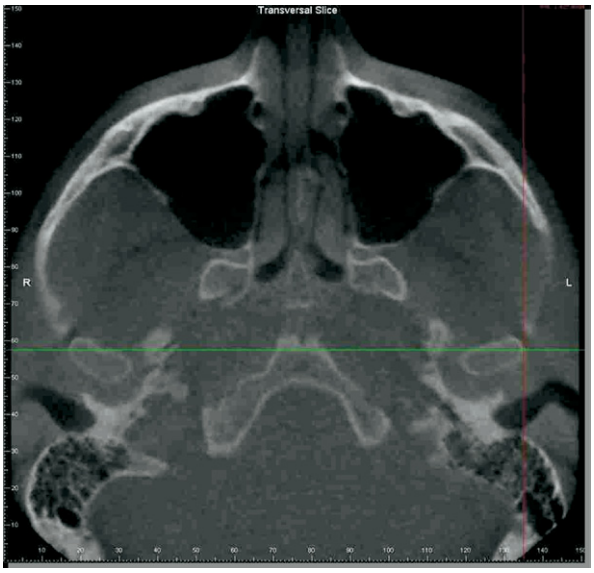

Fig. 2. Selection of 1 plane window display to improve visualization for careful landmark location at each plane at a time. This example displays selection of the axial view in zoom to aid identification of the lateral pole of the left condyle.

was shown in the Y and Z coordinates, as indicated by an ICC of <0.45 for 2 cases (6.66%) in the Y coordinate and 1 case (3.3%) in the Z coordinate, totaling only 3 (3.3%) of all interobserver assessments.

Table IV lists the reliability estimated by ICC for each landmark and each coordinate. Two bilateral landmarks showed low ICC scores, indicative of poor reliability: Y coordinate of right and left ramus, and Z coordinate of right and left condylion.

To further examine the interobserver differences, Table V shows the frequency of differences in mean value on landmark location in the X, Y, and Z coordinates. The frequencies were calculated using the range of mean observer scores in each landmark. The summarized results in Table V illustrate that 69 (76.6%) of the landmarks had a quite small mean difference of ≤1 mm and that in only 2cases (2.22%) did the mean difference exceed 2 mm.

DISCUSSION

Landmark-based analysis using linear and angular measurements are the most popular method of cephalometric analysis among clinicians.[1] Cone-beam CT potentially provides opportunities for 3D cephalometrics in orthodontic assessment of bony landmarks and air-bounded surfaces such as the facial skin.[21] Farman and Scarfe[21] have described methods for creating 2D cephalograms from CBCT volumetric data sets so that direct comparisons can be made between existing 2D databases and the future paradigm of 3D analysis. Just as numerous 2D cephalometric analyses have been proposed since the introduction of the cephalostat by Broadbent, it appears likely that 3D cephalometry will also lead to new definitions of landmarks and new proposed analyses.[2] However, 3D cephalometry requires alterations in paradigms of the 2D radiographic and cephalometric analyses and demands careful training of residents and clinicians to take full advantage of the potential information offered by 3D imaging.

The development of the present study methods required definition of the landmarks in the coronal (anteroposterior) and axial (superior-inferior) planes in addition to the traditional landmark definitions in the sagittal (lateral) plane. The sources of error in landmark identification in this study can be 2-fold. First, some landmarks can be easily identified in 1 or 2 planes of the space, but landmark identification in the third plane might be difficult. Observers tended to locate the landmark in the planes of easy identification, disregarding the plane of difficult visualization. Second, the selection of the best slice for landmark location in each X, Y, and Z coordinate requires time, calibration training, and careful assessment. Three-dimensional landmark identification is more time consuming than conventional 2D cephalograms tracing, because it requires identifying landmarks in coronal, sagittal, and axial views and double-checking the visualization in the 3 planes of the space and in the 3D rendering.

Even though the 3 observers in the present study had different training backgrounds, and 1 of them had no prior experience with CT or CBCT scans, the observers' training background had minimal effect on landmark location errors. This minimal effect of prior experience can be explained by careful observer calibration with the definition of landmark location in each of the 3 planes of space before the start of the study, using a set of 10 CBCT scans not included in the study.

In 2D cephalograms, many landmarks are defined as the uppermost or lowermost point of structures. A point on the edge of a structure in a lateral cephalogram may not correspond to the same point in the coronal cephalogram, owing to the 2 different X-ray beam projections. This absence of spatial correspondence among the 2D views is a problem in 2D cephalograms. But 3D coordinate points correspond to 3D anatomic truth and pinpoint locations in the exact same anatomic locus.[22]

Inherent to 3D landmark-based cephalometric analysis, even in 3D linear and angular analyses, is the limitation of being unable to assess how entire surfaces changed rather than discrete points. Recent studies have reported the use of 3D CBCT virtual surface models instead of the 3D

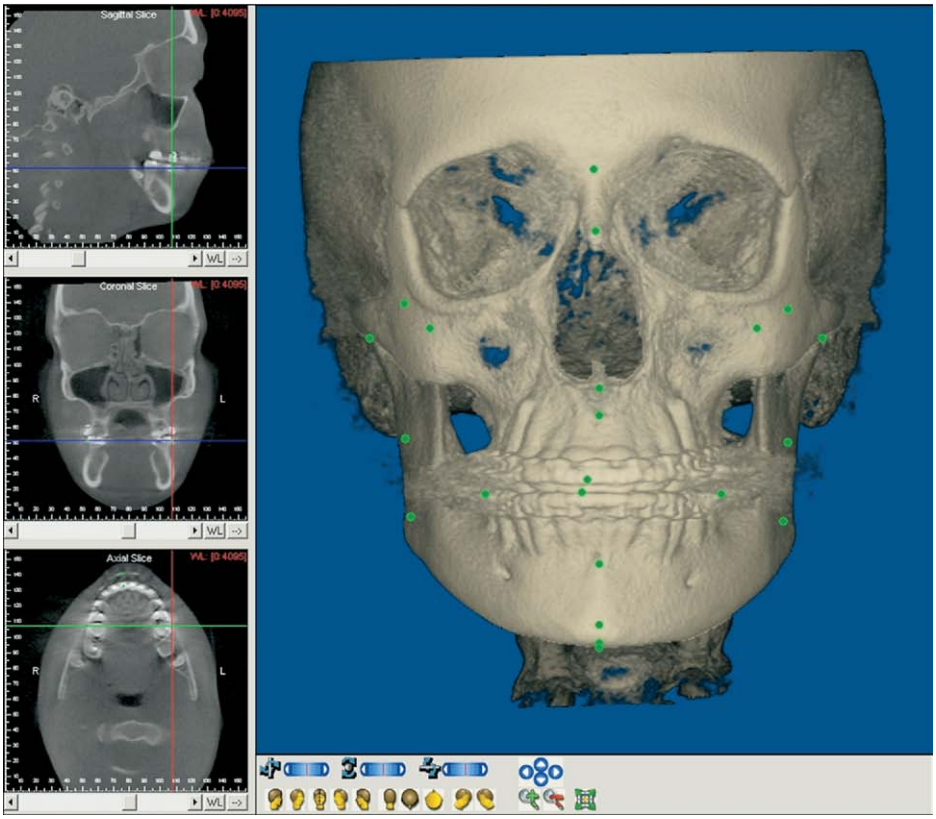

Fig. 3. Landmarks displayed in the 3D rendering. Note that landmark locations appear distorted for landmarks located away from the center of the projected rendered view.

Table II. Frequency of the intraobserver reliability estimated by intraclass correlation (ICC) for the X, Y, and Z coordinates

	Coordinate							
	X		*Y*		*Z*		*Total*	
Range	*n*	*(%)*	*n*	*(%)*	*n*	*(%)*	*n*	*(%)*
ICC ≥ 0.90	24	(80.0)	25	(83.33)	28	(93.33)	77	(85.55)
0.75 < ICC < 0.90	2	(6.66)	3	(10.0)	0	0	5	(5.55)
0.45 < ICC ≤ 0.75	4	(13.33)	2	(6.66)	1	(3.33)	7	(7.77)
ICC ≤ 0.45	0	0	0	0	1	(3.33)	1	(1.11)
Total	30	(100.0)	30	(100.0)	30	(100.0)	90	(100.0)

Table III. Frequency of the inte-observer reliability estimated by intraclass correlations (ICC) for the X, Y, and Z coordinates

	Coordinate							
	X		*Y*		*Z*		*Total*	
Range	*n*	*(%)*	*n*	*(%)*	*n*	*(%)*	*n*	*(%)*
ICC ≥ 0.90	20	(66.6)	15	(50)	24	(80.0)	59	(65.5)
0.75 < ICC < .0.90	4	(13.3)	8	(26.6)	4	(13.3)	16	(17.7)
0.45 < ICC ≤ 0.75	6	(20.0)	5	(16.6)	1	(3.3)	12	(13.3)
ICC ≤ 0.45	0	0	2	(6.6)	1	(3.3)	3	(3.3)
Total	30	(100.0)	30	(100.0)	30	(100.0)	90	(100)

renderings displayed by commercial softwares such as Dolphin and Invivo (Anatomage, San Jose, CA)) for assessment of treatment changes.[6,15,23-25] However, 3D surface models are not available for routine clinical use, because these methods are more time consuming and require computing expertise.

The results of the present study showed that it is possible to accomplish landmark identifications in 3D with a high degree of reliability after training. The greatest frequencies of ICC ≥0.9 were in the axial view in both intra- and interobserver analyses, with 93.3% and 80%, respectively. But overall, the results were satisfactory in all 3 planes of space. One might have expected greatest reproducibility of landmark location in the sagittal (lateral) plane of space, because clinicians are used to landmark identification in 2D lateral

Table IV. Reliability estimated by intraclass correlations for each landmark and each coordinate

	Intraobserver reliability			*Interobserver reliability*		
Landmark	*X*	*Y*	*Z*	*X*	*Y*	*Z*
Anterior nasal spine	0.98	0.99	0.99	0.89	0.83	0.99
A point	0.99	0.94	1	0.91	0.7	0.99
B point	0.98	0.98	1	0.94	0.9	0.99
Gnathion	0.98	0.99	1	0.96	0.92	1
Left Ccondylion	0.66	1	0.5	0.65	0.97	0.49
Left mandibular gonion	0.97	0.92	0.96	0.97	0.73	0.9
Left lower molar point	0.98	0.98	0.93	0.97	0.82	0.87
Left lateral mandibular condyle	0.98	0.98	0.99	0.98	0.94	0.97
Left medial mandibular condyle	0.97	0.98	1	0.97	0.95	0.99
Left orbitale	0.8	0.99	0.99	0.71	0.91	0.93
Left upper molar point	0.97	0.97	1	0.94	0.81	0.95
Left ramus point	0.95	0.68	1	0.94	0.44	0.98
Left tuberosity	0.73	0.75	0.96	0.71	0.57	0.89
Left zygomatic suture	0.92	0.98	0.97	0.86	0.89	0.95
Menton	0.98	1	1	0.95	0.92	1
Nasion	0.99	1	1	0.87	0.98	0.97
Pogonion	0.98	0.99	1	0.96	0.94	1
Right condylion	0.46	0.99	0.29	0.46	0.98	0.28
Right mandibular gonion	0.99	0.89	0.93	0.96	0.71	0.91
Right lower incisal edge	0.99	1	1	0.92	0.88	0.98
Right lower molar point	0.96	0.96	0.93	0.94	0.87	0.88
Right medial mandibular condyle	0.99	0.97	0.99	0.93	0.93	0.99
Right orbitale	0.81	0.99	0.98	0.65	0.96	0.95
Right upper incisal edge	0.98	1	1	0.95	0.79	0.95
Right upper molar point	0.97	0.93	1	0.96	0.85	0.94
Right lateral mandibular condyle	0.99	0.97	0.98	0.97	0.96	0.97
Right ramus point	0.98	0.51	0.99	0.95	0.29	0.99
Right tuberosity	0.73	0.77	0.94	0.71	0.48	0.9
Right zygomatic suture	0.92	0.98	0.96	0.89	0.93	0.95
Sella turcica	0.93	1	1	0.90	0.95	0.99

Table V. Frequency of the difference in mean values on location landmark identification in X, Y, and Z coordinates

	Coordinate							
	X		*Y*		*Z*		*Total*	
Range (mm)	*n*	*(%)*	*n*	*(%)*	*N*	*(%)*	*n*	*(%)*
≥2	0	(0)	0	0	2	(6.6)	2	(2.22)
$1 < x < 2$	6	(20.0)	8	(26.6)	5	(16.6)	19	(21.1)
$0.5 < x \leq 1$	10	(33.3)	13	(43.3)	10	(33.3)	33	(36.6)
≤0.5	14	(46.6)	9	(30.0)	13	(43.3)	36	(40.0)
Total	30	(100)	30	(100)	30	(100)	90	(100)

cephalograms, but observer calibration and training before the present study might have aided reproducibility in all 3 planes of space.[17] Park et al.[4] reported similar results with medical CT, where intraexaminer reliability between 2 observations found that all 19 landmarks used in their study were reproducible, and there was no significant intraexaminer error.

The accuracy and reproducibility of 3D medical CT has been confirmed by Olszewski et al.[26] and Swennen and colleagues,[27,28] but their findings cannot be directly compared with the results in the present study, because they reported inter- and intraobserver reproducibility of cephalometric measurements, not landmark location. Other recent studies described cephalometric analysis based on 3D CT anatomic landmarks to evaluate the craniofacial morphology.[22,26-29] But data acquisition with medical CT has some drawbacks: 1) higher radiation exposure compared with CBCT; 2) horizontal positioning of the patient during record taking falsifies the position of the soft tissue; 3) lack of a detailed occlusion owing to artifacts; and 4) limited access for the routine craniofacial patient, because of higher

cost.[3,4,28,30] The use of 3D medical CT cephalometric analysis might be limited to those complex orthognathic cases with asymmetry and operable craniofacial syndromes.[3,26] The advantages of CBCT over conventional CT include lower radiation dose, lower cost, potentially better access, and high spatial resolution.[3] Although 3D CBCT analysis for diagnosis and treatment still requires clinical validation, it is expected that CBCT 3D cephalometry will soon be available for routine craniofacial care.[28]

Although overall the results of this study were satisfactory in all 3 planes of space, Table IV shows poor reliability of the Y coordinate definition of the right and left ramus points and the Z coordinate of right and left condylion. These findings can be explained by deficient definition criteria of those landmarks in those particular views, and by their location along the anatomic areas that are not areas of maximum curvature. Therefore, the characteristics of the landmark can influence its reproducibility. The choice of landmarks and the ability to reliably identify them determine the usefulness of the 3D cephalometric analysis and have an impact on the accuracy of measurements.[31]

Interobserver mean value differences of X, Y, and Z coordinates in the present study were similar within all 3 planes of space. Sixty-nine (76.6%) of the 90 landmark coordinates had a quite small mean difference of $\leq$1 mm, and in only 2 Z coordinates (2.22%) the mean difference exceeded 2 mm. The clinical significance of the accuracy of the landmark identification error depends on the level of accuracy required. The acceptable degree of error depends on the type and complexity of the treatment procedures being planned and the goals of the study. Other factors related to the accuracy and reliability of 3D landmarks will need to be further investigated, such as the effect of slice thickness, use of overlapping slices, scanning time, gantry tilt, and patient head positioning.[3] The slice thickness used in the present study was 0.3 mm, whereas CT studies use slice thickness of 1 mm or more. Recent studies[4,17] emphasize that narrower slices should result in better measurement accuracy, decreasing the landmark identification errors.

CONCLUSIONS

Overall, the intra- and interobserver reliability was excellent. Three-dimensional landmark identification from CBCT images can offer consistent and reproducible data if a protocol for operator training and calibration is followed. Use of cross-sectional slices in all 3 views of space take full advantage of the 3D CBCT information, although landmark location on the 3D renderings can lead to errors. This is particularly important for landmarks not easily specified in all 3 planes of space.

REFERENCES

1. Kumar V, Ludlow JB, Mol A, Cevidanes L. Comparison of conventional and cone beam CT synthesized cephalograms. Dentomaxillofac Radiol 2007;36:263-9.
2. Halazonetis DJ. From 2-dimensional cephalograms to 3-dimensional computed tomography scans. Am J Orthod Dentofacial Orthop 2005;127:627-37.
3. Lou L, Lagravere MO, Compton S, Major PW, Flores-Mir C. Accuracy of measurements and reliability of landmark identification with computed tomography (CT) techniques in the maxillofacial area: a systematic review. Oral Surg Oral Med Oral Pathol Oral Radiol Endod 2007;104:402-11.
4. Park SH, Yu HS, Kim KD, Lee KJ, Baik HS. A proposal for a new analysis of craniofacial morphology by 3-dimensional computed tomography. Am J Orthod Dentofacial Orthop 2006;129:600.e23-34.
5. Scarfe WC, Farman AG, Sukovic P. Clinical applications of cone-beam computed tomography in dental practice. J Can Dent Assoc 2006;72:75-80.
6. Cevidanes LH, Styner MA, Proffit WR. Image analysis and superimposition of 3-dimensional cone-beam computed tomography models. Am J Orthod Dentofacial Orthop 2006;129:611-8.
7. Hashimoto K, Arai Y, Iwai K, Araki M, Kawashima S, Terakado M. A comparison of a new limited cone beam computed tomography machine for dental use with a multidetector row helical CT machine. Oral Surg Oral Med Oral Pathol Oral Radiol Endod 2003;95:371-7.
8. Hatcher DC, Aboudara CL. Diagnosis goes digital. Am J Orthod Dentofac Orthop 2004;125:512-5.
9. Ito K, Yoshinuma N, Goke E, Arai Y, Shinoda K. Clinical application of a new compact computed tomography system for evaluating the outcome of regenerative therapy: a case report. J Periodontol 2001;72:696-702.
10. Lascala CA, Panella J, Marques MM. Analysis of the accuracy of linear measurements obtained by cone beam computed tomography (CBCT-NewTom). Dentomaxillofac Radiol 2004;33:291-4.
11. Ludlow JB, Davies-Ludlow LE, Brooks SL. Dosimetry of two extraoral direct digital imaging devices: NewTom cone beam CT and Orthophos Plus DS panoramic unit. Dentomaxillofac Radiol 2003;32:229-34.
12. Mah JK, Danforth RA, Bumann A, Hatcher D. Radiation absorbed in maxillofacial imaging with a new dental computed tomography device. Oral Surg Oral Med Oral Pathol Oral Radiol Endod 2003;96:508-13.
13. Mengel R, Candir M, Shiratori K, Flores-de-Jacoby L. Digital volume tomography in the diagnosis of periodontal defects: an in vitro study on native pig and human mandibles. J Periodontol 2005;76:665-73.
14. Mussig E, Wortche R, Lux CJ. Indications for digital volume tomography in orthodontics. J Orofac Orthop 2005;66:241-9.
15. Cevidanes LH, Bailey LJ, Tucker SF, Styner MA, Mol A, Phillips CL, et al. Three-dimensional cone-beam computed tomography for assessment of mandibular changes after orthognathic surgery. Am J Orthod Dentofacial Orthop 2007;131:44-50.
16. Bookstein FL. Morphometric tools for landmark data. Cambridge: Cambridge University Press; 1991. p. 435.
17. Ludlow JB, Laster WS, See M, Bailey LJ, Hershey HG. Accuracy of measurements of mandibular anatomy in cone beam computed tomography images. Oral Surg Oral Med Oral Pathol Oral Radiol Endod 2007;103:534-42.

18. Parrott QW, Mol A. Condylar changes following orthognathic surgery. Thesis submitted to the faculty of the University of North Carolina [Master of Science in the School of Dentistry]. Chapel Hill; 2005.
19. Kumar V, Ludlow J, Cevidanes LHS, Mol A. In vivo comparison of conventional and cone beam CT synthesized cephalograms. Angle Orthodont 2008;78:873-9.
20. Neter J, Kutner MH, Wasserman W, Nachtsheim CJ. Applied linear statistical models. 4th ed. McGraw-Hill/Irwin; 1996. p. 785.
21. Farman AG, Scarfe WC. Development of imaging selection criteria and procedures should precede cephalometric assessment with cone-beam computed tomography. Am J Orthod Dentofacial Orthop 2006;130:257-65.
22. Katsumata A, Fujishita M, Maeda M, Ariji Y, Ariji E, Langlais RP. 3D-CT evaluation of facial asymmetry. Oral Surg Oral Med Oral Pathol Oral Radiol Endod 2005;99:212-20.
23. Cevidanes LH, Bailey LJ, Tucker GR Jr, Styner MA, Mol A, Phillips CL, et al. Superimposition of 3D cone-beam CT models of orthognathic surgery patients. Dentomaxillofac Radiol 2005; 34:369-75.
24. Grauer D, Cevidanes, LHS, Phillips C, Mol A, Styner M, Proffit W. Assessment of maxillary surgery outcomes one year post-surgery, J Dent Res 2006;85(Spec Iss A):813.
25. Lee B, Cevidanes LHS, Phillips C, Mol A, Styner M, Proffit W. 3D assessment of mandibular changes one year after orthognathic surgery. J Dent Res 2006;85(Spec Iss A):1610.
26. Olszewski R, Zech F, Cosnard G, Nicolas V, Macq B, Reychler H. Three-dimensional computed tomography cephalometric craniofacial analysis: experimental validation in vitro. Int J Oral Maxillofac Surg 2007;36:828-33.
27. Swennen GR, Schutyser F, Barth EL, De Groeve P, De Mey A. A new method of 3-D cephalometry Part I: the anatomic cartesian 3-D reference system. J Craniofac Surg 2006;17:314-25.
28. Swennen GR, Schutyser F. Three-dimensional cephalometry: spiral multi-slice vs cone-beam computed tomography. Am J Orthod Dentofacial Orthop 2006;130:410-6.
29. Maeda M, Katsumata A, Ariji Y, Muramatsu A, Yoshida K, Goto S, Kurita K, Ariji E. 3D-CT evaluation of facial asymmetry in patients with maxillofacial deformities. Oral Surg Oral Med Oral Pathol Oral Radiol Endod 2006;102:382-90.
30. Danforth RA, Dus I, Mah J. 3-D volume imaging for dentistry: a new dimension. J Calif Dent Assoc 2003;31:817-23.
31. Baumrind S, Frantz RC. The reliability of head film measurements 1. Landmark identification. Am J Orthod 1971;60:111-27.

Reprint requests:

Lucia H. S. Cevidanes, DDS, MS, PhD
Assistant Professor
Department of Orthodontics
UNC School of Dentistry
201 Brauer Hall
Chapel Hill, NC 27599-7450
cevidanl@dentistry.unc.edu